Open access • Journal Article • DOI:10.1364/OL.37.003723

Spatially incoherent single channel digital Fourier holography — Source link

Roy Kelner, Joseph Rosen

Institutions: Ben-Gurion University of the Negev

Published on: 01 Sep 2012 - Optics Letters (Optical Society of America)

Topics: Digital holography, Digital holographic microscopy, Holography, Digital camera and Fourier transform

Spatially incoherent single channel digital Fourier holography

Roy Kelner* and Joseph Rosen

Department of Electrical and Computer Engineering, Ben-Gurion University of the Negev, P.O. Box 653, Beer-Sheva 84105, Israel
**Corresponding author: kelnerr@post.bgu.ac.il*

Received June 14, 2012; accepted July 16, 2012;
posted July 20, 2012 (Doc. ID 170643); published August 31, 2012

We present a new method for recording digital Fourier holograms under incoherent illumination. A single exposure recorded by a digital camera is sufficient to record a real-valued hologram that encodes the complete three-dimensional properties of an object. © 2012 Optical Society of America

OCIS codes: 090.0090, 090.1995, 110.6880, 100.3010, 070.6120.

In recent years we have witnessed noteworthy achievements of incoherent holography techniques such as optical scanning holography [1] and Fresnel incoherent correlation holography (FINCH) [2,3]. The latter has fundamental system robustness since it is based on a single channel incoherent interferometer and because it does not require any scanning or mechanical movement. However, though a single FINCH image contains the complete three-dimensional (3D) information of an object, at least three images are required to solve the twin image problem [4]. In this Letter, we present a new method for recording digital Fourier holograms under incoherent illumination. Fourier holograms [5,6] possess some advantages over Fresnel holograms including, but not limited to, increased space–bandwidth product performance [7,8] and the relatively easy ability to process and manipulate the hologram, since it is captured in the spatial frequency domain. In addition, the hologram is more robust to information loss, as each object point is distributed over the entire hologram plane. Moreover, by recording a Fourier hologram of a half plane (or space), the twin image problem is avoided and the object can be reconstructed from a single exposure. Still, the proposed method maintains many other advantageous characteristics of FINCH [9]. We coin our method Fourier incoherent single channel holography (FISCH).

The FISCH system is shown in Fig. 1. A white-light source illuminates a 3D object. Light scattered from the object passes through a band pass filter (BPF), becomes partially temporally coherent, and continues to propagate through a single channel incoherent interferometer. Eventually, interference patterns are captured by the CCD. Consider a point source object of complex amplitude A_s positioned at the coordinate (x_s, y_s, z_s), a distance z_s from the lens L_0. A tilted diverging spherical wave of the form $T(x,y;\vec{r}_s,z_s) = A_s c(\vec{r}_s,z_s)L(-\vec{r}_s/z_s)Q(1/z_s)$ is induced over the L_0 plane, where $\vec{r}_s = (x_s, y_s)$, $c(\vec{r}_s,z_s)$ is a complex valued constant dependent on the position of the point source, and $L(\vec{s}) = \exp[i2\pi\lambda^{-1}(s_x x + s_y y)]$ and $Q(s) = \exp[i\pi s\lambda^{-1}(x^2+y^2)]$ are the linear and the quadratic phase functions, respectively, in which λ is defined as the central wavelength. A diffractive optical element of the form $Q(-1/f_1)$ is displayed on the spatial light modulator (SLM), positioned at a small angle relative to the optical axis. The SLM is polarization sensitive, so by introducing the linear polarizer $P1$ the single channel optical apparatus is effectively split into two beams (see [10] for a detailed explanation). With one beam the SLM functions as a converging diffractive lens with a focal length f_1, while in the other it acts as plane mirror. The second polarizer $P2$ rejoins the two beams.

The unmodulated wave at the SLM plane, right after passing through it for the second time, is

$$C_1(x,y;\vec{r}_s,z_s) = T(x,y;\vec{r}_s,z_s)\cdot Q\left(\frac{-1}{f_0}\right) * Q\left(\frac{1}{d_0+2f_1}\right), \quad (1)$$

while the modulated wave, at the same position, is

$$C_2(x,y;\vec{r}_s,z_s) = T(x,y;\vec{r}_s,z_s)\cdot Q\left(\frac{-1}{f_0}\right) * Q\left(\frac{1}{d_0}\right) \cdot Q\left(\frac{-1}{f_1}\right) * Q\left(\frac{1}{2f_1}\right)\cdot Q\left(\frac{-1}{f_1}\right), \quad (2)$$

where $*Q(1/z_d)$ denotes a Fresnel propagation of a wave to a distance of z_d [mathematically, $*$ denotes a two-dimensional (2D) convolution] and $Q(-1/f)$ denotes the influence of a converging lens of focal length f upon a wave propagating through it. Upon arrival to the CCD plane the waves are

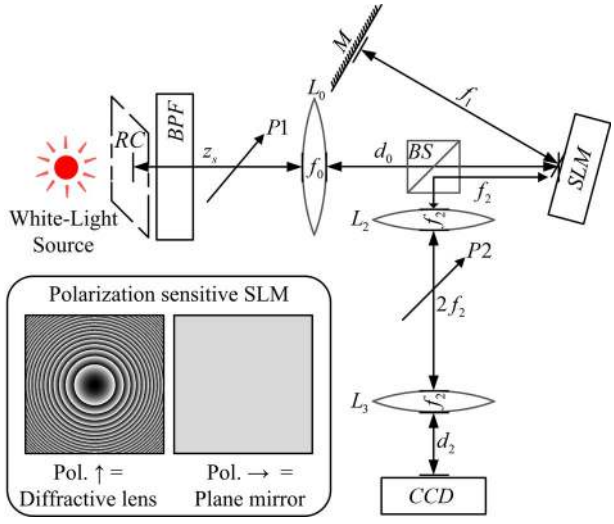

Fig. 1. (Color online) Schematic of a FISCH recorder: RC, resolution chart; BPF, bandpass filter; BS, beam splitter; SLM, spatial light modulator; M, mirror; CCD, charge-coupled device; $P1$ and $P2$, polarizers.

$$D_k(x,y;\vec{r}_s,z_s) = C_k(x,y;\vec{r}_s,z_s) * Q\left(\frac{1}{f_2}\right)\cdot Q\left(\frac{-1}{f_2}\right) * Q\left(\frac{1}{2f_2}\right)\cdot Q\left(\frac{-1}{f_2}\right) * Q\left(\frac{1}{d_2}\right), \quad (3)$$

where $k = 1, 2$ represent the unmodulated and modulated beams, respectively. Following mathematical justification presented in [11], the recorded intensity over the CCD plane, $I(x,y;\vec{r}_s,z_s) = |D_1(x,y;\vec{r}_s,z_s)+D_2(x,y;\vec{r}_s,z_s)|^2$, is equal to

$$I(x,y;\vec{r}_s,z_s) = I_s(|b_1|^2+|b_2|^2) + \left[b_1 b_2^* I_s \cdot L\left(\frac{2\vec{r}_s f_e}{z_s}\cdot\frac{f_3}{f_3^2-4f_1^2}\right)\cdot Q\left(\frac{-4f_1}{f_3^2-4f_1^2}\right)+\text{c.c.}\right], \quad (4)$$

where $I_s = A_s\cdot A_s^*$ is the intensity of the point source, b_1 and b_2 are constants, $f_e = f_0 z_s/(f_0 - z_s)$, $f_3 = f_e + d_0 - f_2 + d_2$ and c.c. is the complex conjugate of the left term inside the square brackets. Since each point source is only spatially coherent to itself, the recorded hologram due to many point sources is simply a summation over all point source contributions. That is, the recorded hologram is

$$H(x,y) = \iiint I(x,y;\vec{r}_s,z_s)\mathrm{d}x_s\mathrm{d}y_s\mathrm{d}z_s. \quad (5)$$

Consider the special case of a point source object positioned at the front focal plane of the lens L_0 (i.e., $z_s = f_0$). In that case, Eq. (4) is easily reduced to

$$I(x,y;\vec{r}_s,f_0) = I_s(|b_1|^2+|b_2|)^2) + \left[b_1 b_2^* I_s\cdot L\left(\frac{2\vec{r}_s}{f_0}\right)+\text{c.c.}\right]. \quad (6)$$

Note that according to the third term of Eq. (6), each source point at $\vec{r}_s$ is mapped at the (x,y) plane to a linear phase with $\vec{r}_s$ dependent inclination and with amplitude dependent on I_s. Such mapping exactly defines a 2D Fourier transform (FT) of the object points. Hence, we have a digital Fourier hologram. Points positioned at the front focal plane of the lens L_0 can be reconstructed by a simple calculation of the inverse FT of $H(x,y)$. Points located on other planes may be out of focus, and can be reconstructed by applying additional Fresnel propagation by the reconstruction distance z_r. The reconstruction procedure (performed either digitally or optically), depicted in Fig. 2 where L_r is a Fourier transforming lens of focal length f_r, gives

$$s(x,y,z_r) = \left(v\left[\frac{1}{\lambda f_r}\right]\mathcal{F}^{-1}\{H(x,y)\}\right) * Q(1/z_r), \quad (7)$$

where $\mathcal{F}^{-1}$ is the inverse FT and v is the scaling operator, which states that $v[a]f(x) = f(ax)$. Based on Eqs. (4) and (7), the reconstruction distance is

$$z_r = \pm 4f_1 f_r^2/(f_3^2 - 4f_1^2). \quad (8)$$

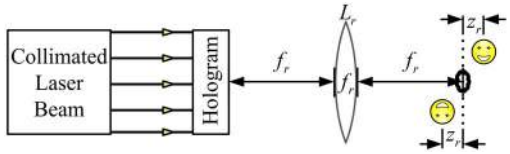

Fig. 2. (Color online) Schematic of the reconstruction apparatus.

According to Eq. (6) and Fig. 2, the reconstruction plane of the point source ($\vec{r}_s, z_s = f_0$) would contain the point source image and its twin, located at ($\pm 2\vec{r}_s f_r/f_0, z_r = 0$), and an additional zeroth order term, located at its origin. Thus, by recording a Fourier hologram the twin image problem is avoided if the object is properly positioned inside a half plane (e.g., $y_s > 0$).

The system shown in Fig. 1 was implemented using a Holoeye PLUTO SLM (1920×1080 pixels, 8 μm pixel pitch, phase only modulation) and a PixelFly CCD (1280×1024 pixels, 6.7 μm pixel pitch, monochrome). Other parameters in the system were $f_0 = 30$ cm, $f_1 = 17.5$ cm, $f_2 = 20$ cm, $d_0 = 13$ cm, and $d_2 = 12$ cm. The resolution test chart (Edmund Optics Negative NBS 1963A) was set at two different z_s positions (30 cm and 25 cm) and was illuminated using a 150 W EKE Halogen lamp light filtered through a 650 ± 20 nm BPF. The intersection angle of the optical axes at the SLM plane was 17°.

We recorded holograms of a single exposure, two exposures, and three exposures. The two latter versions use the phase-shifting method [2,4] to eliminate most of the bias term and, in the three exposures version, also the twin image. Note that the single exposure and two exposures holograms are real-valued, whereas the three exposures hologram is complex-valued. The resulting holograms were digitally reconstructed based on Eq. (7). The real-valued two exposures holograms were also optically reconstructed using an apparatus based on Fig. 2, in which the holograms were displayed on a Holoeye LC2002 SLM (800×600 pixels, 32 μm pixel pitch, set to amplitude modulation through a proper configuration of an input and output polarizers). No special processing was applied to the holograms before displayed on the SLM, besides resizing with accordance to the SLM resolution and linear mapping of the gray levels to discrete values from 0 to 255 (8 bits). This mapping naturally requires the introduction of a bias term, since the two exposure holograms contain both negative and positive real values.

The experimental results are shown in Fig. 3. The first hologram was recorded with the resolution test chart positioned at $z_s = f_0 = 30$ cm. Its reconstructions [Figs. 3(a)–3(d)] are simply the inverse FT of the hologram (discrete transform, in the digital case). Figure 3(a) demonstrates that a single exposure is sufficient for retaining most of the target information. Yet, the zeroth order, clearly visible in the center of the image, dominates the hologram and reduces the quality of the image. Using two exposures [Fig. 3(b)] greatly reduces the bias term, increases the dynamic range of the hologram, and thereby enhances the quality of the image. A third exposure [Fig. 3(c)] removes the twin image, but does not enhance the quality of the image any further, at least not visibly.

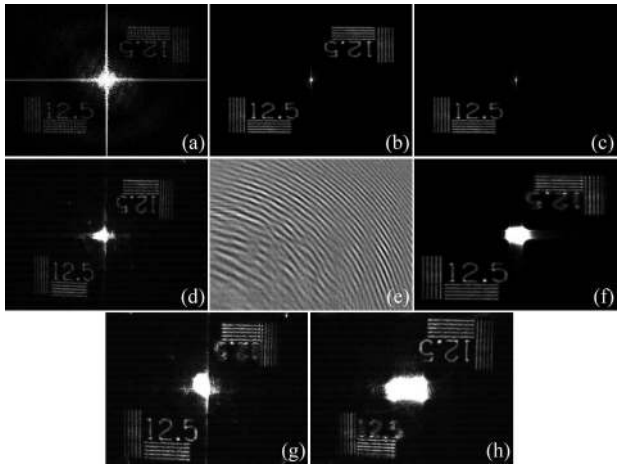

Fig. 3. (a), (b), and (c) are digitally reconstructed images for $z_s = 30$ cm from a single exposure, two and three exposures holograms, respectively; (d) is the optically reconstructed equivalent of (b). (e) is a two exposures hologram (shown partially to reveal details, recorded with $z_s = 25$ cm) and (f) is its digitally reconstructed image at the best plane of focus. (g) and (h) are optical reconstructions of (e) at the best plane of focus of one of the images and its twin, respectively.

Finally, Fig. 3(d) is the optical counterpart of 3(b), and demonstrates the possibility of optical reconstruction of the resulting real-valued hologram using a simple apparatus, as previously described.

To demonstrate the system capability of maintaining 3D information, another hologram was recorded; this time with $z_s = 25$ cm $< f_0$. Part of the recorded hologram (using two exposures) is shown in Fig. 3(e). A digital reconstruction at the best plane of focus is shown in Fig. 3(f), where z_r was calculated according to Eq. (8). The optical reconstructions in Figs. 3(g) and 3(h) clearly demonstrate the refocusing capability of the system, where the image and its twin are in and out of focus, interchangeably. This was simply achieved via back and forth movement of the CCD within the z-axis.

A simplified schematic of FISCH is presented in Fig. 4. We note that in the actual system (Fig. 1) the beams propagate twice through the same SLM, here represented by SLM1 and SLM2. In addition, the CCD is now positioned right after SLM2. This configuration may be considered to be equivalent to Fig. 1 with $d_2 = f_2$, so that the waves reaching the CCD are simply a 180° rotated version of the waves right after exiting the SLM the second time. Here we consider the case of $z_s = f_0$. We further assume that the recorded hologram is limited by a clear disc aperture $P(R_H)$ of radius R_H, which is determined by the overlap area of the two interfering beams on the CCD plane, and that the system is only aperture limited by the radius of SLM1, R_0. In this case, R_H can geometrically be shown to equal R_0, regardless of the source distance from the optical axis, R_S. The recorded hologram is then equal to Eq. (6) multiplied by $P(R_0)$. It can be reconstructed as shown in Fig. 2 so that

$$h(\vec{r}) = v\left[\frac{1}{\lambda f_r}\right]\mathcal{F}^{-1}\{I(x,y;\vec{r}_s,f_0)P(R_0)\}, \qquad (9)$$

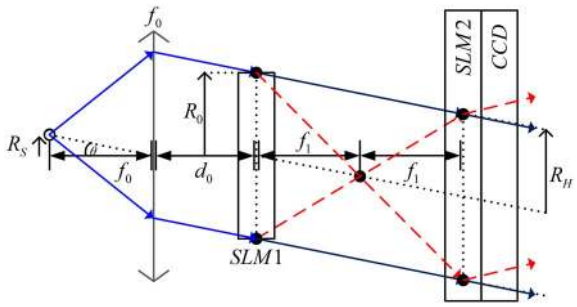

Fig. 4. (Color online) Simplified schematic of a FISCH recorder.

where $\vec{r} = (x, y)$. Equation (9) results with three terms attributed to the bias, the point source image and its twin, which are assumed to be properly separated, once R_S is big enough. The point source image is then proportional to

$$h_F(\vec{r}) \propto J\mathrm{inc}\left(\frac{2\pi R_0}{\lambda f_r}\sqrt{(x - M_T x_s)^2 + (y - M_T y_s)^2}\right), \qquad (10)$$

where $J\mathrm{inc}(r) = J_1(r)/r$, $J_1(r)$ is the Bessel function of the first kind and of order one, and $M_T = (2\vec{r}_s f_r/f_0)/\vec{r}_s = 2f_r/f_0$ is the transverse magnification of the presented FISCH configuration. A comparison of Eq. (10) to Eq. (11) of Ref [9] demonstrates that, under the above conditions, both FISCH and FINCH possess the same point spread function (PSF). Therefore, just like FINCH [9], FISCH has improved resolution beyond the Rayleigh limit when compared to conventional imaging.

In this Letter we have presented FISCH, a new method for recording spatially incoherent digital Fourier holograms. The viability of FISCH and its ability to maintain the complete 3D information of an object were demonstrated. We believe that the combination of FISCH inherent robustness with its capability of recording single exposure holograms under incoherent illumination holds great potential for many possible applications of FISCH.

We thank Barak Katz for sharing his valuable knowledge and experience. This work was supported by the Israeli Ministry of Science and Technology (MOST).

References

1. T.-C. Poon, J. Opt. Soc. Korea **13**, 406 (2009).
2. J. Rosen and G. Brooker, Opt. Lett. **32**, 912 (2007).
3. B. Katz, J. Rosen, R. Kelner, and G. Brooker, Opt. Express **20**, 9109 (2012).
4. I. Yamaguchi and T. Zhang, Opt. Lett. **22**, 1268 (1997).
5. G. W. Stroke and R. C. Restrick, Appl. Phys. Lett. **7**, 229 (1965).
6. J. B. Breckinridge, Appl. Opt. **13**, 2760 (1974).
7. J. W. Goodman, *Introduction to Fourier Optics*, 2nd ed. (McGraw Hill, 1996), Chap. 9, pp. 295–392.
8. D. Claus, D. Iliescu, and P. Bryanston-Cross, Appl. Opt. **50**, H116 (2011).
9. J. Rosen, N. Siegel, and G. Brooker, Opt. Express **19**, 26249 (2011).
10. G. Brooker, N. Siegel, V. Wang, and J. Rosen, Opt. Express **19**, 5047 (2011).
11. B. Katz and J. Rosen, Opt. Express **18**, 962 (2010).